Nanoscale

PAPER

View Article Online
View Journal | View Issue

Cite this: *Nanoscale*, 2023, **15**, 18818

Band structure sensitive photoresponse in twisted bilayer graphene proximitized with WSe_2†

Aparna Parappurath, *[a] Bhaskar Ghawri,[a] Saisab Bhowmik,[b] Arup Singha,[a] K. Watanabe, [c] T. Taniguchi[d] and Arindam Ghosh[a,e]

Received 26th September 2023,
Accepted 8th November 2023

DOI: 10.1039/d3nr04864k

rsc.li/nanoscale

The ability to tune the twist angle between different layers of two-dimensional (2D) materials has enabled the creation of electronic flat bands artificially, leading to exotic quantum phases. When a twisted blilayer of graphene (tBLG) is placed at the van der Waals proximity to a semiconducting layer of transition metal dichalcogenide (TMDC), such as WSe_2, the emergent phases in the tBLG can fundamentally modify the functionality of such heterostructures. Here we have performed photoresponse measurements in few-layer-WSe_2/tBLG heterostructure, where the mis-orientation angle of the tBLG layer was chosen to lie close to the magic angle of 1.1°. Our experiments show that the photoresponse is extremely sensitive to the band structure of tBLG and gets strongly suppressed when the Fermi energy was placed within the low-energy moiré bands. Photoresponse could however be recovered when Fermi energy exceeded the moiré band edge where it was dominated by the photogating effect due to transfer of charge between the tBLG and the WSe_2 layers. Our observations suggest the possibility of the screening effects from moiré flat bands that strongly affect the charge transfer process at the WSe_2/tBLG interface, which is further supported by time-resolved photo-resistance measurements.

Owing to exceptional band tunability, twisted bilayer graphene (tBLG) has emerged as an ideal system to study various interaction-driven phases such as correlated insulators,[1] superconductivity,[1,2] magnetism,[3–5] non-Fermi liquids[6,7] and non-trivial band topology.[8,9] More recently, it has been shown that tBLG proximitized with a layer of WSe_2 can not only lead to orbital ferromagnetism[10] but also the broken symmetry states at half-integer fillings.[11] Although different transport measurements have shed light on the rich-phase diagram of WSe_2/tBLG devices, the understanding of light–matter interaction in such systems remains elusive as previous experiments in this direction are limited only to twisted graphene layers[12–14] or twisted layers of transition metal dichalcogenides.[15] It has been demonstrated and well established that photoresponse in single-layer graphene enhances by orders of magnitude when proximitized with TMDC, owing to the efficient charge separation at the heterostructure interface and the photogating effect.[16–21] Probability of charge transfer across the interface is dictated by the availability of electronic states at the Fermi energy of graphene[16] and the tunability of photoresponse characteristics of conventional graphene integrated heterostructures is limited by the linear band dispersion.[16,22] With the emergence of flat band electronics, the photoresponse measurements on tBLG/TMDC heterostructures could hence open up new avenues to explore the rich physics in tBLG.

In this work, we demonstrate photoresponse in tBLG proximitized with few-layer WSe_2. We identify strong photoresponse *via* photogating when the Fermi energy is located beyond the moiré band edge. Surprisingly however, we observe a complete suppression of photoresponse as the Fermi level is tuned inside the low-energy moiré band at low temperatures. Since the twist angles of our different measurement channels are close to the magic angle (1.17°), we speculate the role of screening effects from moiré flat bands in the observed photoresponse. Our results are further validated by detailed time-

[a]*Department of Physics, Indian Institute of Science, Bangalore, 560012, India. E-mail: aparnap@iisc.ac.in, arindam@iisc.ac.in*
[b]*Department of Instrumentation and Applied Physics, Indian Institute of Science, Bangalore, 560012, India*
[c]*Research Center for Functional Materials, National Institute for Materials Science, Namiki 1-1, Tsukuba, Ibaraki 305-0044, Japan*
[d]*International Center for Materials Nanoarchitectonics, National Institute for Materials Science, Namiki 1-1, Tsukuba, Ibaraki 305-0044, Japan*
[e]*Centre for Nano Science and Engineering, Indian Institute of Science, Bangalore 560 012, India*

†Electronic supplementary information (ESI) available: Device fabrication and measurement methods, discussion on flat bands in WSe_2 proximitized tBLG, Band filling factor estimation, transport data from different measurement channels, photoresponse data from different measurement channel, photoresponse measurements on control device, calculation for conduction band threshold of WSe_2, Photoresponse and dR/dn magnitude variation as a function of temperature, photoresponse and dR/dn comparison at higher temperature, variation of photoresponsivity with optical power density. See DOI: **https://doi.org/10.1039/d3nr04864k**

resolved photoresponse measurements where the device is exposed to successive light on–off pulses while maintaining the back gate voltage at a constant value.

A schematic of the tBLG/WSe_2 heterostructure device used for photoresponse measurements is shown in Fig. 1a. The measurement channel consists of few-layer WSe_2 proximitized tBLG encapsulated by bottom and top hBN layers. The desired vertical heterostructure is assembled using a dry transfer technique involving the tear and stack method reported in ref. 11 and 23. The stack is etched to Hall bar geometry, and Ohmic edge contacts are defined by e-beam lithography followed by Cr/Au (5/50 nm) thermal evaporation. Fermi energy level and hence the number density of tBLG channel is tuned using a Si^{++}/SiO_2 back gate. Details of electrical transport and optoelectronic measurements are presented in ESI-I.†

To characterize the transport properties of the device, four terminal longitudinal resistance (R) is measured as a function of back gate voltage (V_{BG}) at different temperatures and presented in Fig. 1b. At the lowest temperature of T = 12 K, we observe the maxima of R appearing at the charge neutrality point (CNP) and two prominent side peaks emerging on either side of the CNP that correspond to the full filling of moiré band ($\nu = \pm 4$) (see ESI-II† for general discussion on flat bands in WSe_2 proximitized tBLG and ESI-III† for band filling factor and angle estimation). While the peaks at $\nu = \pm 4$ show insulating behaviour throughout the measured temperature range, at the CNP we observe resistance increases with increasing temperature till 150 K and then decreases with increasing temperature up to 293 K. From the position of side peaks, we calculate the effective twist angle $\theta \approx 1.17° \pm 0.03$. The transport data for

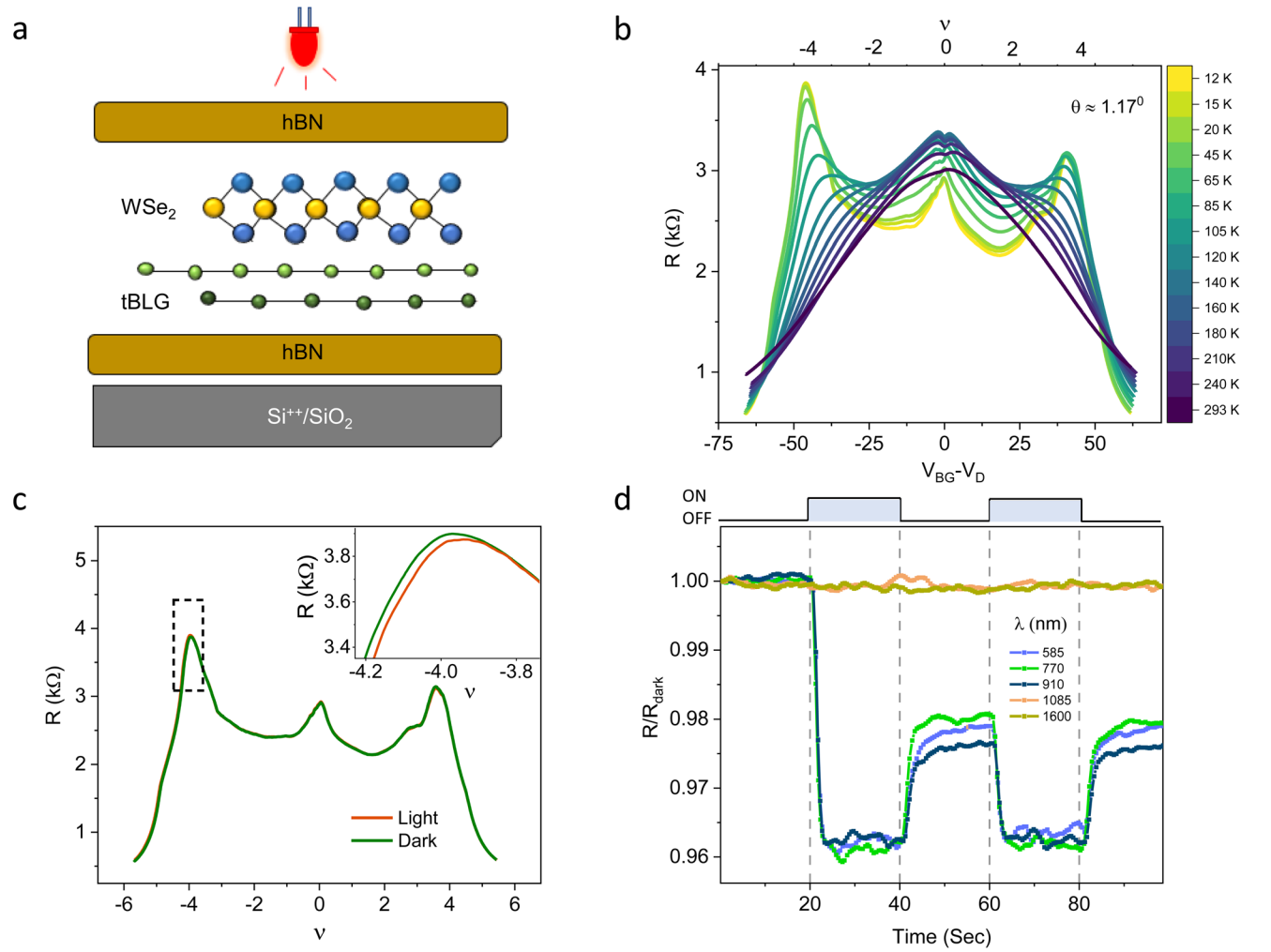

Fig. 1 Schematic and device characterization (a) Schematic of hBN-encapsulated tBLG-WSe_2 heterostructure for electrical and optoelectronic measurements. (b) Four-probe resistance R as a function of filling factor ν measured at different temperatures between 12 K and 293 K. (c) R as a function of ν in the absence (green) and presence (orange) of light with λ = 585 nm and T = 12 K. The inset shows the zoomed in region near $\nu = -4$ (marked by dashed rectangle), where photoresponse is most prominent. (d) Normalized resistance (R/R_{dark}) as a function of time when device is illuminated with two consecutive light on–off pulses keeping the Fermi level at $\nu = -4.6$. The experiments are repeated with five different wavelengths ranging from 585 nm to 1600 nm.

other measurement channels with twist angles $\theta \approx 1.17° \pm 0.02$ and $\theta \approx 1.14° \pm 0.02$ are presented in ESI-IV.†

Next, we present the preliminary optoelectronic characterization of the device. In Fig. 1c, we compare channel resistance as a function of band filling factor under dark (green trace in Fig. 1c) and continuous light (light emitting diode (LED) wavelength 585 nm, power density 155 fW μm^{-2}) illumination conditions (orange trace in Fig. 1c). A difference is observed between light on and off resistance values when the Fermi level is tuned to $|\nu| > 4$ (see inset of Fig. 1c). At $\nu = -4.26$, we further perform the typical time-resolved photoresponse of the device under the light-on–off pulses of wavelengths ranging from 585 nm to 1600 nm (Fig. 1d). The absence of photoresponse above 910 nm *i.e*, photon energy below WSe_2 bandgap, confirms that photo carriers are generated in WSe_2 upon light illumination.[24–26] The observed negative photoresponse (decrease in resistance on light illumination) in the hole side further suggests the transfer of holes from WSe_2 to tBLG, leading to a photogating effect in the system.[16] However, our observation of hole transfer from WSe_2 to tBLG is in contrast to the previously reported photo-electron transfer in graphene/TMDC heterostructures.[27,28] We attribute this to the inverse stacking order of tBLG/WSe_2 layers in our device geometry, where the direction of the applied gate electric field is reversed at the heterostructure interface, as we elucidate later in detail.

We show the sensitivity of photoresponse to tBLG band structure in Fig. 2. The photo-resistance ($\Delta R = R(n)_{ON} - R(n)_{OFF}$) is compared with dR/dn in Fig. 2a. We observe that the photoresponse follows dR/dn with a sign reversal when the Fermi level is below moiré edge in the valence band. The $-dR/dn$ trend further confirms hole transfer mediated photogating dominating in the heterostructure.

Surprisingly, it is observed that the response is greatly suppressed when the Fermi level is tuned inside moiré band ($|\nu| < 4$). Importantly, the suppression of photoresponse inside the moiré band is consistent in all other contact configurations irrespective of the enhanced dR/dn near the CNP (see ESI-V†). We also present the photoresponse magnitude ($\Delta R = R_{ON} - R_{OFF}$) as a function of ν calculated from pulsed light on–

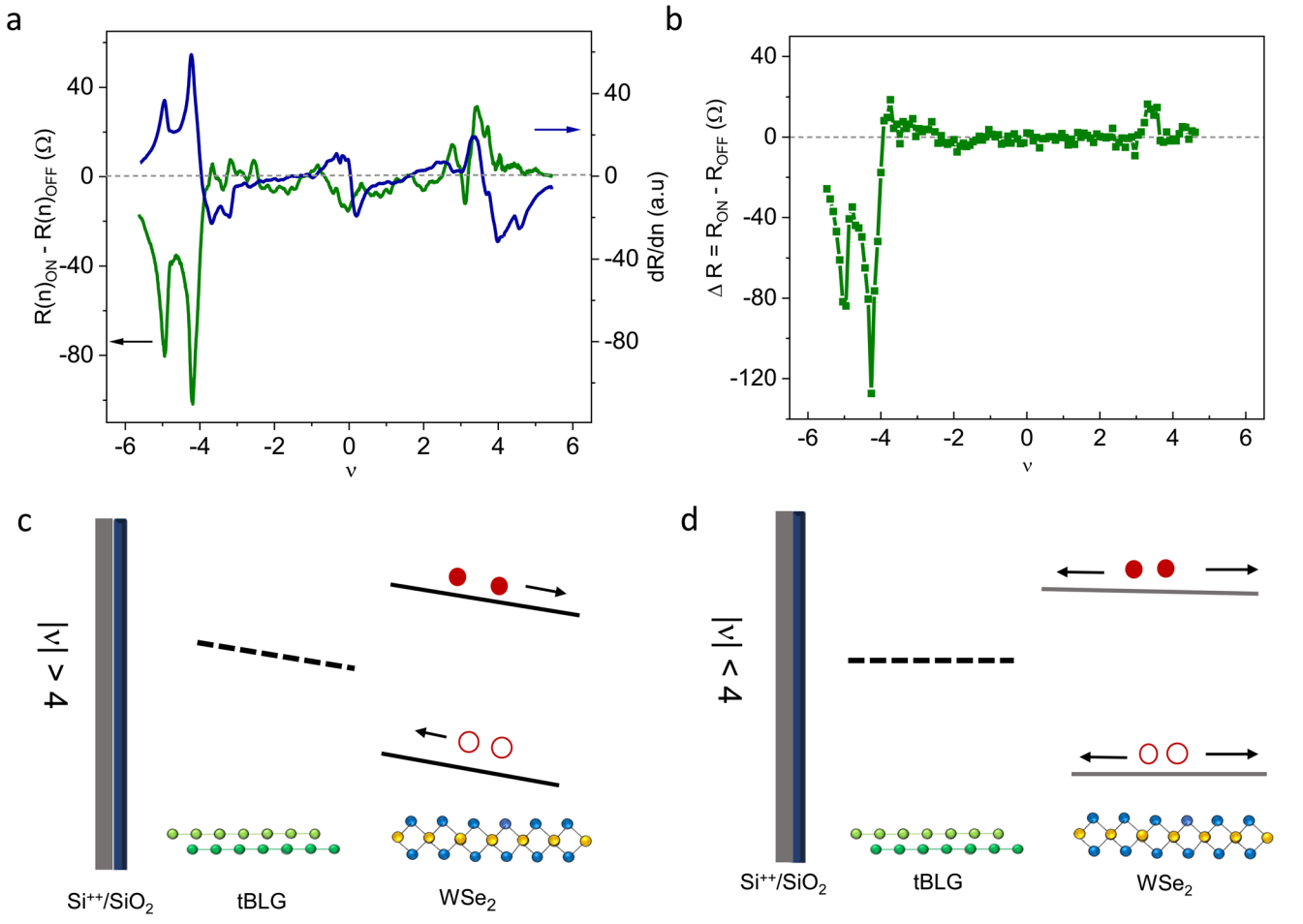

Fig. 2 Gate voltage dependence of the photoresponse (a) Comparison between $R(n)_{ON} - R(n)_{OFF}$ (left axis) and dR/dn (right axis) at 12 K with λ = 585 nm suggesting photogating as the prominent mechanism of photoresponse. $R(n)_{OFF}$ is the off-state (dark state) resistance and $R(n)_{ON}$ is the On-state resistance under continuous light illumination. (b) Photo-resistance $\Delta R = R_{ON} - R_{OFF}$ as a function of ν extracted from pulsed lighton-off measurements. (c and d) Schematics depicting the charge transfer process at the interface for $|\nu| > 4$ (c) and $|\nu| < 4$ (d).

off measurements performed at discrete gate voltages in Fig. 2b and note that the photoresponse features are repeated in both continuous and pulsed illumination measurements. For $|\nu| > 4$, the Fermi level in tBLG is tuned to the superlattice band gap, and the channel is expected to behave as an insulator in this regime.[23] Hence the applied negative electric field from the back gate through tBLG could effectively separate the photo-generated carriers in WSe_2 and favour hole transfer, as depicted in Fig. 2c. The insulating nature of the tBLG channel in this gate voltage window can also be verified from the temperature-dependent resistance measurements presented in Fig. 1b and ESI-IV.† As we tune the Fermi level to $|\nu| < 4$, the photo carrier dynamics and hence the response are crucially influenced by the low-energy moiré bands. The high density of states (DoS) in these bands can effectively screen the applied back gate voltage from WSe_2. We speculate that the screening effect hampers the efficiency of uni-directional hole transfer at the interface as the WSe_2 bands remain flat in this gate voltage window. The inefficient charge separation leading to vanishing photoresponse inside the low-energy moiré bands is schematically presented in Fig. 2d. We also note that the photoresponse characteristics in TMDC based photo-detectors are susceptible to interfacial effects.[29,30] In order to rule out the effect from interface and trap states associated with WSe_2 in the observed photoresponse behavior, we perform control experiments on hBN/WSe_2/bilayer graphene device and present in ESI-VI.† Electric field-assisted charge transfer and the photogating mediated photoresponse are observed throughout the measured gate voltage window in a bilayer graphene-based device. Hence we confirm that the suppression of photoresponse is a unique signature of tBLG arising from the flat bands.

The screening effect inside low-energy moiré bands is captured further in the time-resolved photoresistance measurements presented in Fig. 3. For $|\nu| > 4$, we observe persistence in photoresistance (*i.e*, the channel resistance not recovering back to the dark state after the illumination is turned off) as reported in graphene/TMDC heterostructures previously.[16,17,20,27,31] Application of a gate voltage pulse above TMDC conduction threshold is the conventional approach to recover the system back to pre-illumination condition.[16] However, here we apply a series of gate pulses ranging from −50 V to −15 V and observe the extent of recovery at $\nu = -4.6$ ($V_{BG} = -55$ V), following the application of each gate pulse. The persistence is quantified in terms of recovery percentage as shown in Fig. 3a. We plot the recovery percentage as a function of the applied gate pulse for two different measurement channels in Fig. 3b. An increase in recovery is observed with the gate pulse pushing the Fermi level far inside the moiré flat band. Interestingly, the resistance recovers back to its pre-illumination dark state value as the Fermi energy reaches close to $\nu \sim 1.5$ (corresponds to a gate pulse of −15 V where the Fermi level is expected below the conduction threshold of WSe_2 as shown in ESI-VII†). The observations imply that carrier recombination is restricted mainly because of the applied field direction. As the Fermi level is tuned deep inside the band, the screening effect weakens the field, allowing the charge distribution to equilibrate throughout the hybrid.

We extend our measurements further to higher temperatures, as presented in Fig. 4. The temperature dependence of photoresistance is compared with that of dR/dn for $|\nu| > 4$ (Fig. 4a and b). The sensitivity of dR/dn to temperature is perfectly captured in photoresistance measurements. The reduction in the response magnitude with temperature, strictly

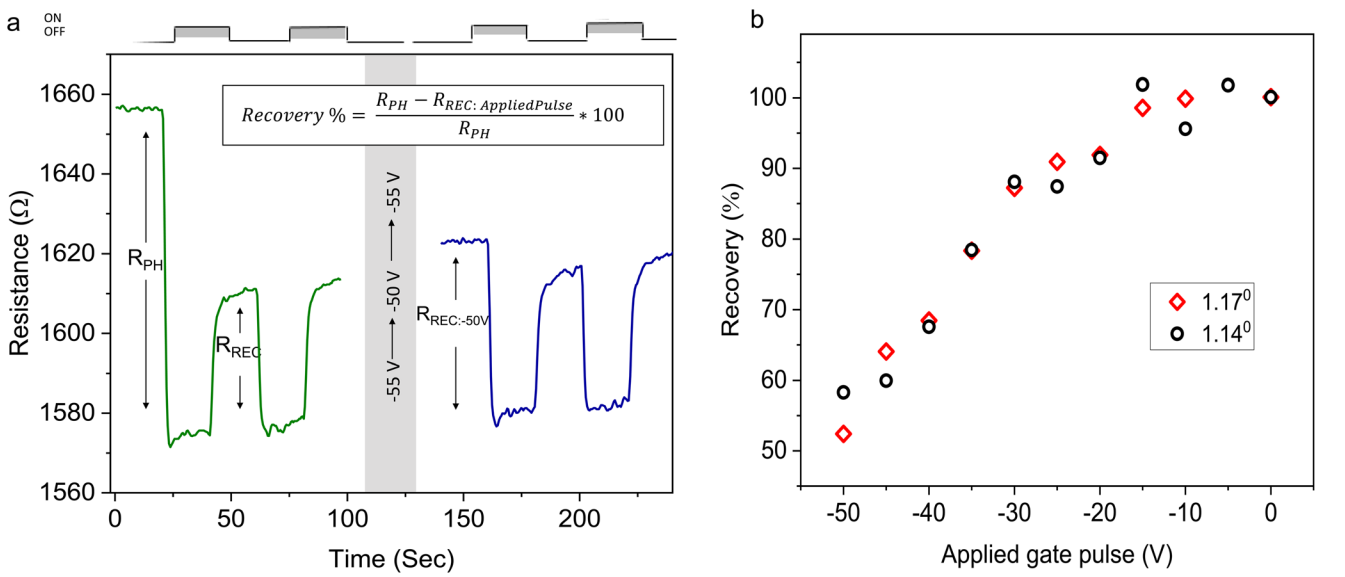

Fig. 3 Persistence and reset operation (a) The time resolved photoresponse showing persistence at $V_{BG} = -55$ V ($\nu = -4.6$). Photo resistance and recovery resistance are marked as R_{PH} and R_{REC} respectively. (b) Recovery percentage calculated as function of the applied gate pulse from time resolved measurements performed at $\nu = -4.6$.

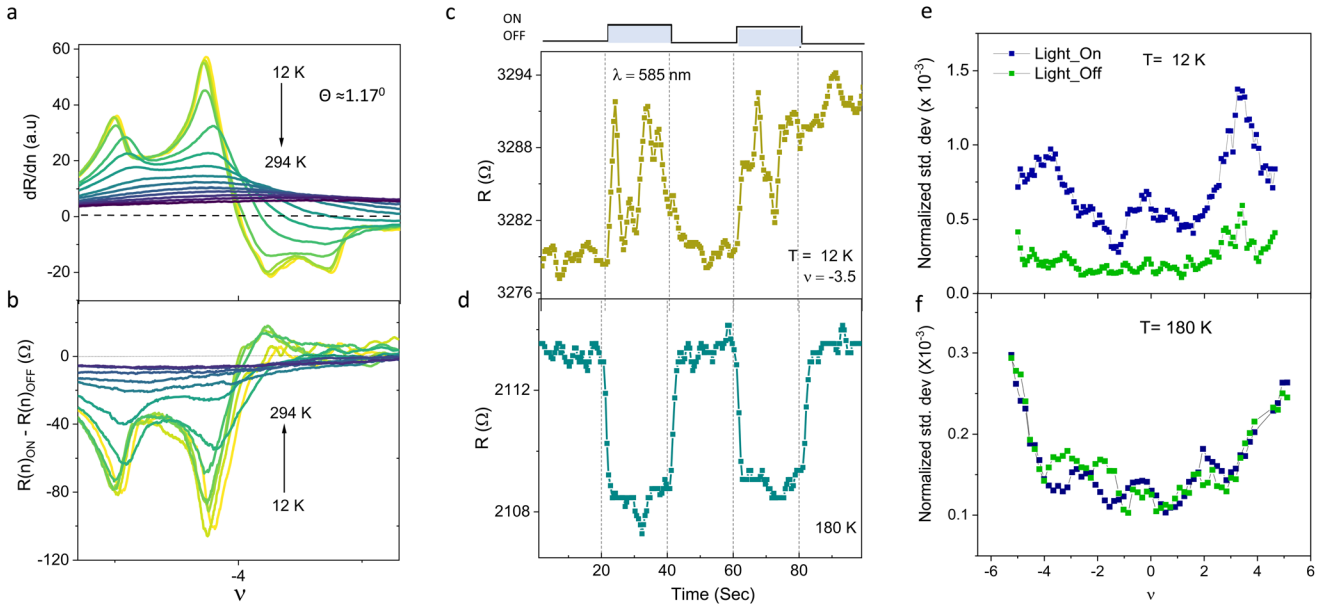

Fig. 4 Temperature dependence of photoresponse (a) The derivative of R as a function of ν for different temperatures in the vicinity of $\nu = -4$. (b) Change in R as a function of ν for different temperatures when the device is illuminated with a light of wavelength $\lambda = 585$ nm. (c and d) R as a function of time at $\nu = -3.5$ for $\lambda = 585$ nm and $T = 12$ K and 180 K respectively. (e and f) Normalized standard deviation plotted as function of ν for temperatures $T = 12$ K (e) and $T = 180$ K (f) under light on and off conditions.

following the trend in dR/dn magnitude (ESI-VIII†), suggests that photogating remains the dominant mechanism throughout the measured temperature range for $|\nu| > 4$. Interestingly, we observe clear photoresponse for $|\nu| < 4$ with increasing temperature, and note a deviation from the dR/dn trend, which is discussed in the context of bolometric effect in ESI ESI-IX† following the references.[13,32] The time-resolved photoresponse at $\nu = -3.5$ is presented at two different temperatures of $T = 12$ K and $T = 180$ K in Fig. 4c and d. We observe that irrespective of the small magnitude, the response becomes clearly distinguishable from the noise level at elevated temperatures. With increasing thermal energy, the carriers at the moiré edge get access to higher bands. This effectively reduces the carrier density and screening in the flat bands allowing the electric field from the back gate to be effective at the heterostructure interface. We anticipate that the effective applied gate electric field, along with the thermal smearing of DoS, make the charge transfer at the interface efficient at elevated temperatures.

Adding further to the interest, in Fig. 4c and d we note that the large fluctuations in resistance that could effectively mask the small photoresponse at low temperatures decrease with increasing temperature. We analyze the noise magnitude under the light on and off conditions at different temperatures to understand this effect further.

The noise magnitude is estimated using the normalized standard deviation in resistance under light on and off pulse of 20 seconds duration each. We plot the normalized standard deviation (std. dev) as a function of filling factor and observe an overall enhancement in noise magnitude under light on condition at 12 K (Fig. 4e). We observe that the difference in noise under on and off conditions is most pronounced near the band edge, and gradually decreases on both sides of $|\nu| = 4$. The difference however becomes undetectable at higher temperature (Fig. 4f). The large noise at $|\nu| = 4$ in the presence of light seems to suggest a light-assisted McWhorter-like number fluctuation noise,[33–35] due to stochastic charge exchange between the tBLG and the WSe_2 layers. Within this framework, the noise magnitude is determined by the correlated number-mobility fluctuation, which sharply increases at $|\nu| = 4$ because of the suppression of screening when the Fermi energy is located within the moiré gap. Both the decrease in the absolute magnitude of ON-state noise, as well as the difference between the noise in the ON and OFF states, suggests that time scales of light-assisted back (tBLG to WSe_2) and forth (WSe_2 to tBLG) charge transfer at the interface shortens with increasing temperature and extends well beyond the bandwidth of our experiments. The reduction in back transfer time scale with increasing temperature in graphene/TMDC heterostructure has been reported previously[20] where it is attributed to the thermally activated back transfer of photogenerated charge carriers at the interface. We speculate that the shortening of forward transfer timescales results from the electric field assisted charge transfer from WSe_2 to tBLG as the screening effect diminishes with increasing temperature.

We also want to highlight that by proximitizing tBLG with WSe_2, the photo responsivity reaches a value of 10^9 V W^{-1} in our device (see ESI-X†). This value is orders of magnitude higher than the responsivity reported for bolometric-originated photoresponse in BLG and tBLG devices.[12,36] Photogating being the dominating mechanism in the current device architecture, such an enhancement is naturally

expected owing to the high photoconductive gain.[29,37] The enhanced responsivity allows the system to be optically probed with low illumination power, bypassing any heating effects. Hence our observations open the possibility of further optoelectronic investigations employing polarized light and magnetic field to probe exotic physics emerging in WSe_2 proximitized tBLG system where maintaining ultra-low temperatures is an essential requirement.

Finally, we comment on the electron–hole asymmetry prominently observed in the photoresponse (Fig. 2). The intrinsic electron–hole asymmetry in WSe_2 proximitized tBLG band structure is well established.[10,11,38] Theoretical calculations on BLG/WSe_2 heterostructures show that the low-energy valence bands in BLG originate from the non-dimer carbon atom orbitals in the graphene layer adjacent to WSe_2, while the conduction band is formed by non-dimer orbitals in other layer.[39] It leads to a larger overlap between wave functions of WSe_2 and the graphene orbitals in the valence band as compared to the conduction band, which can affect the charge transfer efficiency. We speculate that this asymmetry in orbital overlap leads to larger photoresponse observed in valence bands compared to the conduction band. Although the theoretical predictions were made for BLG, we believe a similar effect should also be valid for tBLG. Another possibility for electron–hole asymmetry can arise from the asymmetry in the dispersiveness of higher energy valence and conduction bands that can have pronounced differences in screening effect in the two cases; however, there is no clear theoretical or experimental evidence for this.

In conclusion, we show that photoresponse in tBLG proximitized by WSe_2 is highly sensitive to the tBLG band structure. We demonstrate photogating effects in the tBLG layer prevailing above moiré band edge, while strong suppression of photoresponse is observed as the Fermi level is tuned inside moiré flat bands. To our knowledge there is no known platform based on 2D materials where such sharp variation in optoelectronic sensitivity could be observed across a band edge. The absence of photoresponse within the low energy moire bands is identified as a unique property of the tBLG arising from the "flatness" of the bands that causes greater screening. We propose a charge transfer model accounting for the screening effects from moiré carriers, thereby capturing photoresponse's sensitivity to tBLG band structure. By proximitizing tBLG with WSe_2 we also observe photo responsivity enhancing by orders of magnitude in comparison to the bolometric-originated photoresponse in tBLG reported previously. This further opens up the possibility of employing this device architecture to optically probe spin–orbit coupling and other low-temperature effects, which would have been impractical otherwise due to the high-power optical light illumination requirements and the associated heating effects.

Conflicts of interest

The authors declare no competing interests.

Acknowledgements

The authors acknowledge financial support from U.S. Army International Technology Centre Pacific (ITC-PAC) and Ministry of Electronic and Information Technology (MEITy), Govt. of India. A. P. thanks Ministry of Education, Govt. of India for the Prime Minister's Research Fellowship (PMRF). Authors would like to acknowledge Dr U Chandni for providing infrastructure for heterostrcuture assembly. We would like to thank Navkiranjot Kaur Gill, Aniket Majumdar and Dr Saloni Kakkar for helpful discussions. K. W. and T. T. acknowledge support from JSPS KAKENHI (Grant Numbers 19H05790, 20H00354 and 21H05233).

References

1 Y. Cao, *et al.*, Unconventional superconductivity in magic-angle graphene superlattices, *Nature*, 2018, **556**, 43.
2 X. Lu, *et al.*, Superconductors, orbital magnets and correlated states in magic-angle bilayer graphene, *Nature*, 2019, **574**, 653–657.
3 M. Serlin, *et al.*, Intrinsic quantized anomalous hall effect in a moiré heterostructure, *Science*, 2020, **367**(6480), 900–903.
4 A. L. Sharpe, *et al.*, Emergent ferromagnetism near three-quarters filling in twisted bilayer graphene, *Science*, 2019, **365**, 605–608.
5 C. Tschirhart, *et al.*, Imaging orbital ferromagnetism in a moiré chern insulator, *Science*, 2021, **372**, 1323–1327.
6 Y. Cao, *et al.*, Strange metal in magic-angle graphene with near Planckian dissipation, *Phys. Rev. Lett.*, 2020, **124**, 076801.
7 B. Ghawri, *et al.*, Breakdown of semiclassical description of thermoelectricity in near-magic angle twisted bilayer graphene, *Nat. Commun.*, 2022, **13**, 1–7.
8 K. P. Nuckolls, *et al.*, Strongly correlated chern insulators in magic-angle twisted bilayer graphene, *Nature*, 2020, 1–6.
9 S. Wu, Z. Zhang, K. Watanabe, T. Taniguchi and E. Y. Andrei, Chern insulators, van Hove singularities and topological flat bands in magic-angle twisted bilayer graphene, *Nat. Mater.*, 2021, **20**, 488–494.
10 J.-X. Lin, *et al.*, Spin-orbit–driven ferromagnetism at half moiré filling in magic-angle twisted bilayer graphene, *Science*, 2022, **375**, 437–441.
11 S. Bhowmik, *et al.*, Broken-symmetry states at half-integer band fillings in twisted bilayer graphene, *Nat. Phys.*, 2022, 1–5.
12 B. Deng, *et al.*, Strong mid-infrared photoresponse in small-twist-angle bilayer graphene, *Nat. Photonics*, 2020, **14**, 549–553.
13 S. Hubmann, *et al.*, Infrared photoresistance as a sensitive probe of electronic transport in twisted bilayer graphene, *2D Mater.*, 2022, **10**, 015005.

14 W. Xin, *et al.*, Photovoltage enhancement in twisted-bilayer graphene using surface plasmon resonance, *Adv. Opt. Mater.*, 2016, **4**, 1703–1710.
15 X. Wang, *et al.*, Light-induced ferromagnetism in moiré superlattices, *Nature*, 2022, **604**, 468–473.
16 K. Roy, *et al.*, Graphene–MoS_2 hybrid structures for multifunctional photoresponsive memory devices, *Nat. Nanotechnol.*, 2013, **8**, 826–830.
17 S. Mitra, S. Kakkar, T. Ahmed and A. Ghosh, Graphene-WS_2 van der Waals hybrid heterostructure for photodetector and memory device applications, *Phys. Rev. Appl.*, 2020, **14**, 064029.
18 S. Sett, A. Parappurath, N. K. Gill, N. Chauhan and A. Ghosh, Engineering sensitivity and spectral range of photodetection in van der Waals materials and hybrids, *Nano Express*, 2022, **3**(1), 014001.
19 H. Fang and W. Hu, Photogating in low dimensional photodetectors, *Adv. Sci.*, 2017, **4**, 1700323.
20 A. Parappurath, *et al.*, Interlayer charge transfer and photodetection efficiency of graphene–transition-metal-dichalcogenide heterostructures, *Phys. Rev. Appl.*, 2022, **17**, 064062.
21 D.-H. Park and H. C. Lee, Photogating effect of atomically thin graphene/MoS_2/$MoTe_2$ van der waals heterostructures, *Micromachines*, 2023, **14**, 140.
22 R. R. Nair, *et al.*, Fine structure constant defines visual transparency of graphene, *science*, 2008, **320**, 1308–1308.
23 Y. Cao, *et al.*, Superlattice-induced insulating states and valley-protected orbits in twisted bilayer graphene, *Phys. Rev. Lett.*, 2016, **117**, 116804.
24 P. R. Pudasaini, *et al.*, High-performance multilayer WSe_2 field-effect transistors with carrier type control, *Nano Res.*, 2018, **11**, 722–730.
25 W. Zhao, *et al.*, Origin of indirect optical transitions in few-layer MoS_2, WS_2, and WSe_2, *Nano Lett.*, 2013, **13**, 5627–5634.
26 W. Zhao, *et al.*, Evolution of electronic structure in atomically thin sheets of WS_2 and WSe_2, *ACS Nano*, 2013, **7**, 791–797.
27 R. Kashid, *et al.*, Observation of inter-layer charge transmission resonance at optically excited graphene-tmdc interfaces, *APL Mater.*, 2020, **8**, 091114.
28 T. Ahmed, K. Roy, S. Kakkar, A. Pradhan and A. Ghosh, Interplay of charge transfer and disorder in optoelectronic response in graphene/hBN/MoS_2 van der waals heterostructures, *2D Mater.*, 2020, **7**, 025043.
29 M. M. Furchi, D. K. Polyushkin, A. Pospischil and T. Mueller, Mechanisms of photoconductivity in atomically thin MoS_2, *Nano Lett.*, 2014, **14**, 6165–6170.
30 P.-H. Chen, *et al.*, Passivated interfacial traps of monolayer MoS_2 with bipolar electrical pulse, *ACS Appl. Mater. Interfaces*, 2023, **15**, 10812–10819.
31 S. Kakkar, *et al.*, High-efficiency infrared sensing with optically excited graphene-transition metal dichalcogenide heterostructures, *Small*, 2022, **18**, 2202626.
32 A. Majumdar, *et al.*, Probing the charge and heat transfer channels in optically excited graphene–transition metal dichalcogenide hybrids using johnson noise thermometry, *Appl. Phys. Lett.*, 2022, **121**, 041103.
33 A. N. Pal, *et al.*, Microscopic mechanism of 1/f noise in graphene: Role of energy band dispersion, *ACS Nano*, 2011, **5**, 2075–2081.
34 P. Karnatak, T. Paul, S. Islam and A. Ghosh, 1/f noise in van der waals materials and hybrids, *Adv. Phys.: X*, 2017, **2**, 428–449.
35 M. A. Aamir and A. Ghosh, Electrical noise inside the band gap of bilayer graphene, *2D Mater.*, 2019, **6**, 025018.
36 J. Yan, *et al.*, Dual-gated bilayer graphene hot-electron bolometer, *Nat. Nanotechnol.*, 2012, **7**, 472–478.
37 G. Konstantatos, *et al.*, Hybrid graphene–quantum dot phototransistors with ultrahigh gain, *Nat. Nanotechnol.*, 2012, **7**, 363–368.
38 H. S. Arora, *et al.*, Superconductivity in metallic twisted bilayer graphene stabilized by WSe_2, *Nature*, 2020, **583**, 379–384.
39 M. Gmitra and J. Fabian, Proximity effects in bilayer graphene on monolayer wse_2: field-effect spin valley locking, spin-orbit valve, and spin transistor, *Phys. Rev. Lett.*, 2017, **119**, 146401.